Highly Active, Selective, and Reusable RuO$_2$/SWCNT Catalyst for Heck Olefination of Aryl Halides

Mayakrishnan Gopiraman,[†] Ramasamy Karvembu,*[,‡] and Ick Soo Kim*[,†,§]

[†]Nano Fusion Technology Research Lab, Interdisciplinary Graduate School of Science and Technology, Shinshu University, Ueda, Nagano 386 8567, Japan

[‡]Department of Chemistry, National Institute of Technology, Tiruchirappalli 620 015, India

[§]Division of Frontier Fibers, Institute for Fiber Engineering (IFES), Interdisciplinary Cluster for Cutting Edge Research (ICCER), National University Corporation, Shinshu University, Ueda, Nagano 386 8567, Japan

ⓢ *Supporting Information*

ABSTRACT: Very fine RuO$_2$ nanoparticles (RuO$_2$NPs) with a mean diameter of about 0.9 nm were decorated on single-walled carbon nanotubes (SWCNTs) by a straightforward "dry synthesis" method. TEM images and the Raman spectrum of the resultant material (RuO$_2$/SWCNT) revealed excellent adhesion and homogeneous dispersion of the RuO$_2$NPs on anchoring sites of the SWCNTs. The surface area of RuO$_2$/SWCNT was found to be 416 m^2 g^{-1}. The SEM−EDS results showed that the weight percentage of Ru in RuO$_2$/SWCNT was 13.8%. The oxidation state of Ru in RuO$_2$/SWCNT was +4, as confirmed by XPS and XRD analyses. After the complete characterization, a 0.9 mol % loading of RuO$_2$/SWCNT was used as a nanocatalyst for the Heck olefination of a wide range of aryl halides to yield products in excellent yields with good turnover numbers and turnover frequencies. Less reactive bromo- and chloroarenes were also used for the formation of coupled products in good yields. RuO$_2$/SWCNT is regioselective, chemoselective, heterogeneous in nature, and reusable. The stability of RuO$_2$/SWCNT was also studied by means of TEM, ICP-MS, SEM−EDS, and XPS analyses.

KEYWORDS: single-walled carbon nanotubes, ruthenium dioxide nanoparticles, heterogeneous nanocatalyst, Heck olefination, regioselectivity, reusability
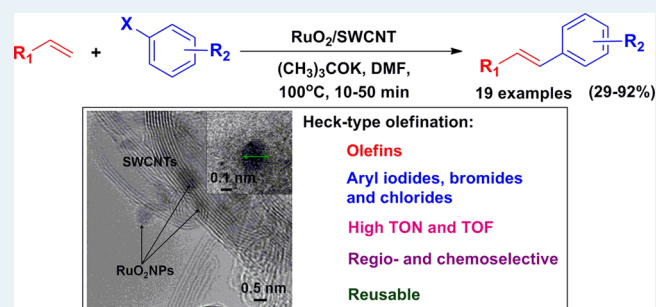
1. INTRODUCTION

The transition-metal-catalyzed C−C cross-coupling reaction is a key step in the synthesis of organic building blocks, natural products, pharmaceuticals, and agricultural derivatives.[1] Certainly, Pd-catalyzed olefination of aryl halides (the Heck−Mizoroki reaction) is one of the most powerful tools for the construction of C−C bonds.[2] In fact, the Pd-based catalytic systems are highly efficient, and they generally offer excellent product yields with good selectivity.[3] To date, several Pd-based homogeneous and heterogeneous catalytic systems have been proposed for the Heck coupling reaction. Among them, because of their high activity, easy separation, stability, and reusability, Pd nanoparticles (PdNPs), particularly supported PdNPs, have gained vast importance.[4] Mehnert et al.[5a] prepared a PdNP-grafted mesoporous MCM-41 material (Pd-TMS11) by a vapor deposition method and used it as a heterogeneous catalyst for Heck reactions. They concluded that the Pd-TMS11 catalyst is highly active, easily accessible, and exceptionally stable. Similarly, Ioni et al.[5b] found that PdNPs decorated on a carbon support such as graphene oxide showed higher activity for the Heck−Mizoroki reaction. Although the PdNP-based catalytic systems are highly dominant, recently the

use of NPs formed from other metals such as Cu,[6] Ni,[7] Fe,[8] Rh,[9] and Ir[10] have been reported for the Heck-type olefination of aryl halides. In fact, from an economical point of view, these metal NPs (excluding Rh and Ir) are much cheaper and more reusable than supported PdNPs. For instance, Houdayer et al.[11a] reported an inexpensive and highly efficient polyaniline/NiNP nanocatalyst for the Heck coupling reaction. Recently, Miao and co-workers[11b] found that composites consisting of RhNPs and PtNPs supported on polymeric hollow latex spheres are efficient for coupling reactions. In spite of their good catalytic activity in Heck coupling reactions, the scope and functional group tolerance of these catalytic systems are generally limited. More importantly, they show less effectiveness in the Heck olefination of less-active bromo- and chloroarenes. In addition, most of the catalytic systems suffer from the use of higher metal loadings (typically 5−10 mol %) and poor reusability. Therefore, the development of an efficient catalytic system for Heck-type olefination is a challenging task.
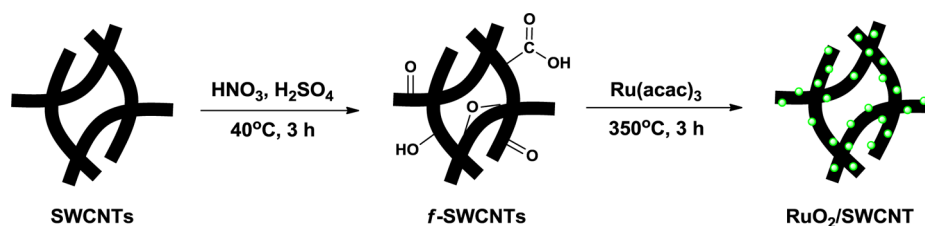
Figure 1. Schematic illustration of the preparation of RuO₂/SWCNT.

Because of its wide range of oxidation states (−2 to +8) and tunable properties, Ru metal has shown the ability to catalyze a remarkable range of organic transformations.[12] Particularly, in the past few years RuNP-catalyzed cross-coupling reactions were found to be an effective tool for the construction of C−C bonds.[13] Na et al.[14] employed a Ru/Al₂O₃ catalyst for both Heck olefination and Suzuki coupling reactions. They found that the Ru/Al₂O₃ catalyst is highly effective and reusable but that bromo- and chloroarenes are less reactive. Hence, there is a continuous exploration for a better heterogeneous Ru-based catalytic system for the Heck coupling reaction. According to Joo et al.,[15a] the activity of a supported metal NPs catalyst is dependent on three main factors: (i) the nature of the support, (ii) the metal−support interactions, and (iii) the particle size. Indeed, single-walled carbon nanotubes (SWCNTs) are one of the promising supports for active metal catalysts in heterogeneous catalysis, and they are trustable because of their astounding properties such as high specific surface area and chemical as well as electrochemical inertness.[16] Recently, Krasheninnikov et al.[17] demonstrated that inert SWCNTs can be transformed to a very active catalyst through interactions between active metal clusters and carbon vacancies. We presumed that the decoration of very fine RuO₂NPs could transform SWCNTs to a very active catalyst for the Heck olefination reaction. In this study, ultrafine RuO₂NPs were decorated over SWCNTs by a simple "dry synthesis" method, and the resulting material, termed RuO₂/SWCNT, was used as a nanocatalyst for the Heck olefination of aryl halides. The regioselectivity and chemoselectivity of the RuO₂/SWCNT-catalyzed Heck olefination reaction were investigated, and the heterogeneity, reusability, and stability of RuO₂/SWCNT were also examined.

2. EXPERIMENTAL SECTION

2.1. Materials and Characterization.
SWCNTs (purity >90% with >70% of the carbon as SWCNTs) with diameters ranging from 0.7 to 1.3 nm were purchased from Sigma-Aldrich and used as received. All other chemicals were purchased from Sigma-Aldrich or Wako Pure Chemicals (Osaka, Japan).

The surface morphology of RuO₂/SWCNT was investigated by transmission electron microscopy (TEM) on a JEOL JEM-2100F high-resolution transmission electron microscope at an accelerating voltage of 200 kV. To quantify the weight percentage of Ru in RuO₂/SWCNT, scanning electron microscopy−energy-dispersive X-ray spectroscopy (SEM−EDS) was performed using a Hitachi 3000H scanning electron microscope. The same field of view was then scanned using an EDS spectrometer to acquire a set of X-ray maps for Ru, C, and O using 1 ms point acquisition for approximately 1 million counts. A Raman spectrometer (Hololab 5000, Kaiser Optical Systems, Inc., Ann Arbor, MI, USA) was applied to examine the interaction between RuO₂NPs and SWCNTs. The Ar laser was operated at 532 nm with a Kaiser holographic edge filter. X-ray

diffraction (XRD) experiments were performed at room temperature using a Rotaflex RTP300 diffractometer (Rigaku Co., Tokyo, Japan) operated at 50 kV and 200 mA. Nickel-filtered Cu Kα radiation (5° < 2θ < 80°) was used for XRD measurements. X-ray photoelectron spectroscopy (XPS) was performed on a Kratos Axis-Ultra DLD spectrometer (Kratos Analytical Ltd., Manchester, U.K.) to confirm the oxidation state of Ru in RuO₂/SWCNT. During the XPS analysis, the sample was irradiated with a Mg Kα X-ray source. Fourier transform infrared (FT-IR) spectra were recorded on KBr pellets at room temperature using a NEXUS 670 FT-IR spectrophotometer (Thermo Nicolet Co., Madison, WI, USA) in the range of 500−4000 cm⁻¹. The conversions of the reactants and the yields of coupled products were determined using a Shimadzu GC-2014 gas chromatograph. The heterogeneity of the RuO₂/SWCNT was tested using inductively coupled plasma-mass spectrometry (ICP-MS) (Agilent 7500CS). NMR spectra were recorded on a Bruker 400 MHz NMR spectrometer using tetramethylsilane (TMS) as a standard.

2.2. Dry Synthesis of RuO₂/SWCNT.
Functional groups such as C=O, COOH, C−OH, and C−O−C are very important anchoring sites for metal NPs that assist in homogeneous decoration and good adhesion of metal NPs on SWCNTs.[18a] Hence, at first, SWCNTs were treated with acid. In a typical procedure, 1.0 g of SWCNTs was chemically treated with a 3:1 mixture of conc. H₂SO₄ (75 mL) and HNO₃ (25 mL), and then the mixture was sonicated at 40 °C for 3 h in an ultrasonic bath. After cooling to 21 °C, the solution mixture was diluted with 1000 mL of deionized water and then vacuum-filtered through filter paper of 0.65 μm porosity. The resultant solid (f-SWCNTs) was washed with deionized water until the pH became neutral and then dried in vacuo at 60 °C. After that, 0.13 g of Ru(acac)₃ was added to 0.5 g of f-SWCNTs and mixed well using a mortar and pestle. A homogeneous mixture of f-SWCNTs and Ru(acac)₃ was obtained in 13−15 min. Finally, the mixture was calcined under a nitrogen atmosphere at 350 °C for 3 h in a muffle furnace. Figure 1 shows a schematic illustration of the procedure for the preparation of RuO₂/SWCNT.

2.3. Procedure for the Heck Olefination Reaction.
In a typical procedure, RuO₂/SWCNT (5 mg, 0.9 mol %) was added to a mixture of styrene (343 μL, 3.0 mmol), iodobenzene (111 μL, 1.0 mmol), and (CH₃)₃COK (224 mg, 2.0 mmol) in DMF, and the resulting mixture was stirred at 100 °C for 10 min. The progress of the reaction was monitored by thin-layer chromatography (TLC) and gas chromatography (GC). After the completion of reaction, the RuO₂/SWCNT was separated from the reaction mixture via centrifugation, and then the separated nanocatalyst was washed well with ethyl acetate followed by diethyl ether and dried in an oven at 60 °C for 5 h. On the other hand, the centrifugate was partitioned between 15 mL of ethyl acetate and 10 mL of saturated aqueous sodium
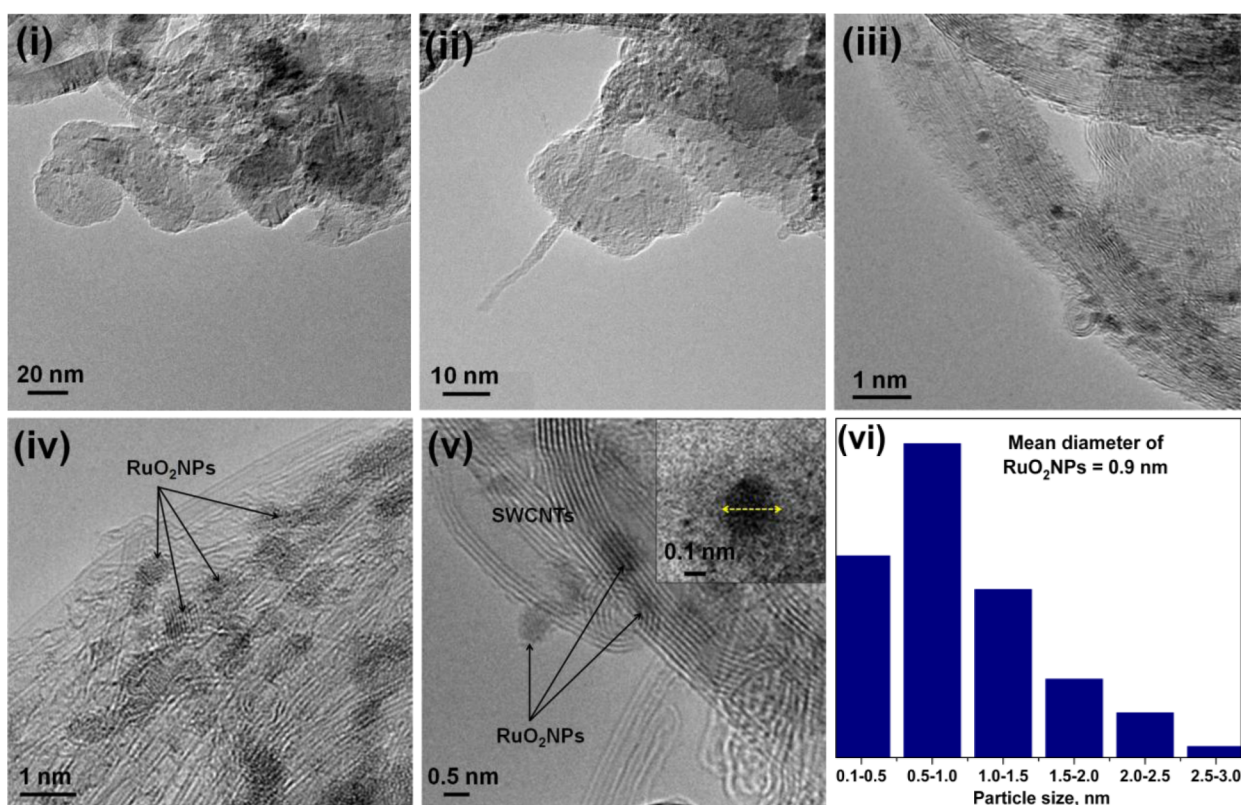
Figure 2. (i, ii) Low- and (iii−v) high-magnification HRTEM images of RuO$_2$/SWCNT and (vi) the particle size distribution of RuO$_2$NPs in RuO$_2$/SWCNT.
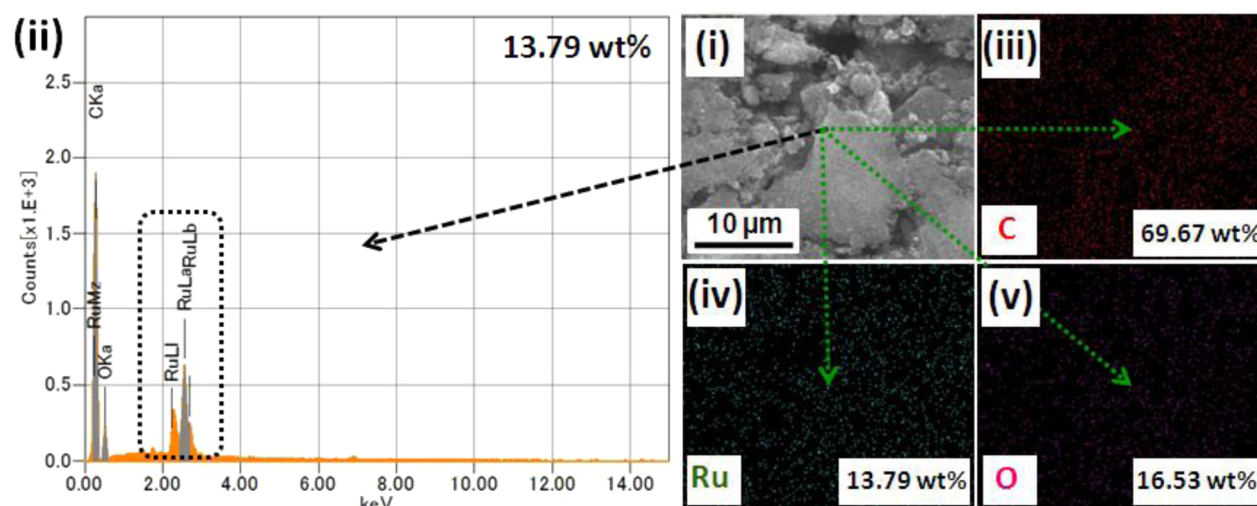

Figure 3. (i) SEM image and (ii) EDS spectrum of RuO$_2$/SWCNT and corresponding EDS mappings of (iii) C, (iv) Ru, and (v) O.

hydrogen carbonate. Subsequently, the organic layer was separated out and dried over anhydrous magnesium sulfate. The yield of olefinated product was determined by GC. Finally, the organic layer was concentrated to obtain the coupled product. The products were confirmed by ^{1}H and ^{13}C NMR spectra.

2.4. Product Analyses. In order to confirm the formation of the products, samples of both reactants and products were dissolved in ethyl acetate and then analyzed by GC. The gas chromatograph was equipped with a Restek 5% diphenyl/95% dimethylsiloxane capillary column (0.32 mm diameter, 60 m in length) and a flame ionization detector (FID). He gas was used

as the carrier gas. The initial column temperature was increased from 60 to 150 °C at a rate of 10 °C/min and then to 280 °C at a rate of 40 °C/min. During the product analyses, the temperatures of the FID and injection port were kept constant at 150 and 280 °C, respectively.

3. RESULTS AND DISCUSSION

3.1. Characterization of RuO$_2$/SWCNT. Figure 2 shows the high-resolution TEM (HRTEM) images of RuO$_2$/SWCNT and the particle size distribution histogram of RuO$_2$NPs in RuO$_2$/SWCNT. As shown in Figure 2i−v, very fine and homogeneously dispersed RuO$_2$NPs were externally attached
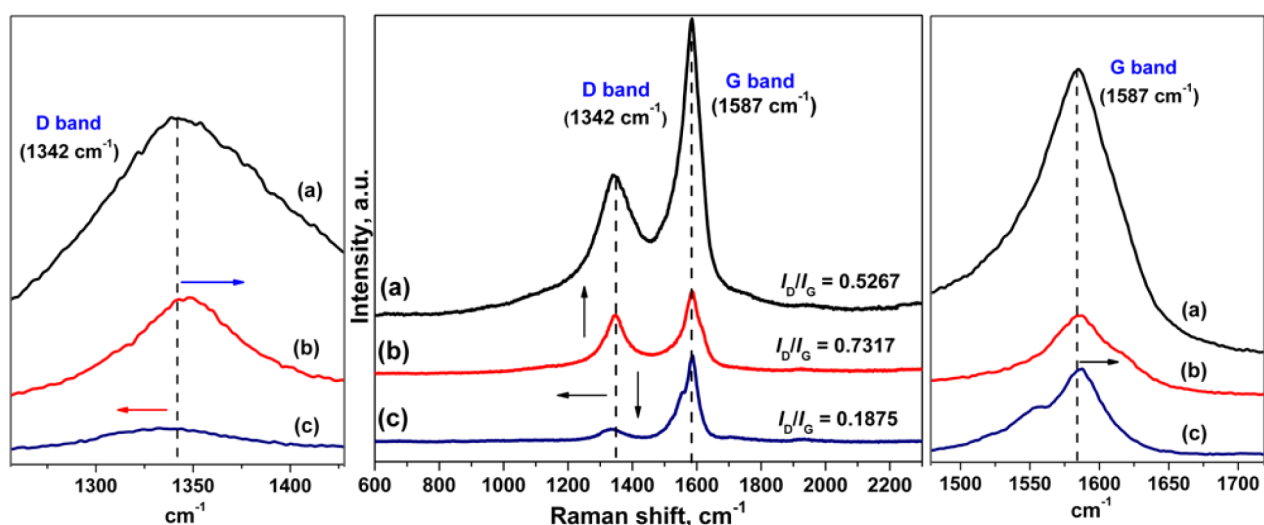
Figure 4. (center) Raman spectra of (a) pure SWCNTs, (b) *f*-SWCNTs, and (c) RuO$_2$/SWCNT. (left) Magnified D band region. (right) Magnified G band region.
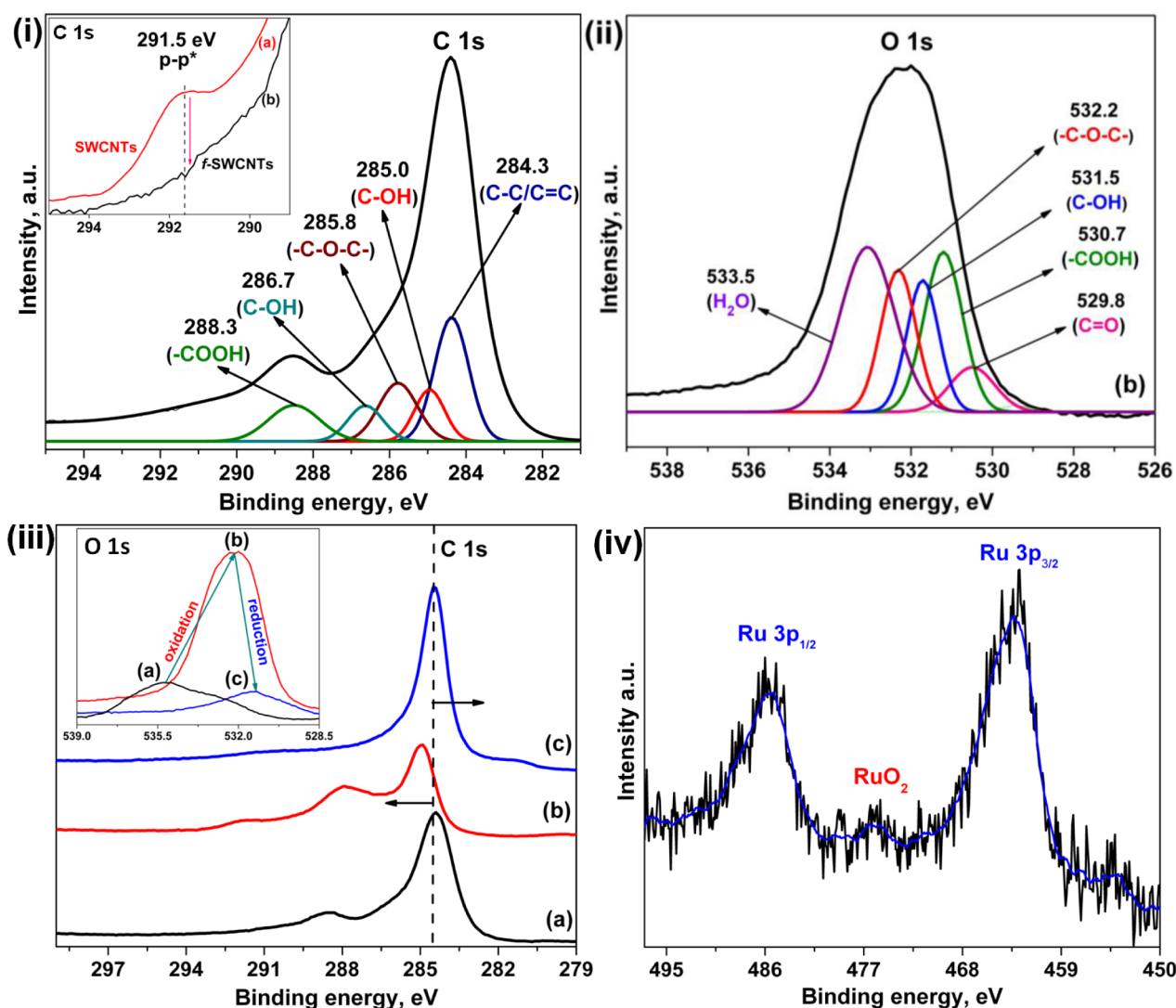

Figure 5. (i) C 1s peak of *f*-SWCNTs. (ii) O 1s peak of *f*-SWCNTs. (iii) C 1s peaks and (inset) O 1s peaks of (a) SWCNTs, (b) *f*-SWCNTs, and (c) RuO$_2$/SWCNT. (iv) Main Ru 3p peaks of RuO$_2$/SWCNT.

on anchoring sites of the SWCNTs (for more details, refer to the TEM images shown in Figure S1 in the Supporting Information). The homogeneous dispersion of RuO_2NPs in RuO_2/SWCNT was also confirmed by HRTEM elemental mapping of Ru (see Figure S2 in the Supporting Information). The size distribution histogram of RuO_2NPs revealed that the diameter of the RuO_2NPs ranged from 0.1 to 3.0 nm with a mean diameter of 0.9 nm (Figure 2vi). It is worth mentioning that no free RuO_2NPs were observed in the background of the TEM images, which shows complete utilization of the RuO_2NPs by the SWCNTs. RuO_2/SWCNT has a Brunauer−Emmett−Teller (BET) surface area of 415.74 m^2 g^{-1} with a pore volume of 0.6541 cm^3 g^{-1} and a Barrett−Joyner−Halenda (BJH) desorption average pore diameter of 1.2 nm. These values are slightly lower than those of f-SWCNTs (BET surface area = 461.51 m^2 g^{-1}, pore volume = 0.8194 cm^3 g^{-1}, and BJH average pore diameter = 1.5 nm) as a result of the incorporation of the RuO_2NPs on the SWCNTs. Moreover, the theoretical specific surface area (i.e., the surface area per unit mass) of RuO_2NPs was calculated to be $S = 956.5$ m^2 g^{-1} using the equation $S_{calcd} = 6000/(\rho d)$,[15b] where d is the mean diameter and ρ is the density of RuO_2 (6.97 g cm^{-3}). According to Bartholomew et al.,[4j] maximizing the S value of catalytic NPs obviously enhances the number of active sites per unit mass upon which catalytic reactions can occur via chemisorption of the substrates. The weight percentage of Ru in RuO_2/SWCNT was 13.79 wt %, as determined by SEM−EDS analysis (Figure 3i,ii). Figure 3iv,v shows the homogeneous distribution of RuO_2NPs in RuO_2/SWCNT. RuO_2/SWCNT contains only the elements C, Ru, and O, as shown by EDS analysis (Figure 3iii−v), which indicates the reliability of the proposed method. Since a trace amount (5−15 ppm) of metal impurities such as Pd may also catalyze the Heck reaction,[3] the possible presence of metal impurities (mainly Pd impurities in RuO_2/SWCNT) was investigated by ICP-MS analysis. RuO_2/SWCNT was found to be free from metal impurities, including Pd (0 ppb). The detection limit of Pd species by ICP-MS is ∼5 ppt.[18b]

To investigate the interaction of RuO_2NPs on SWCNTs, Raman spectra were recorded for pure SWCNTs, f-SWCNTs, and RuO_2/SWCNT over the Raman shift interval of 200−4000 cm^{-1} (spectra a−c, respectively, in Figure 4). All three samples showed two characteristic peaks at 1345 and 1592 cm^{-1} corresponding to the sp^3- and sp^2-hybridized carbons, respectively, confirming the presence of disordered graphite (D band) and ordered-state graphite (G band) in the SWCNTs.[19] Since the ratio of the intensities of the D and G bands (I_D/I_G) is often used as a diagnostic tool to measure the defect concentration in SWCNTs, the I_D/I_G ratio was calculated for all three samples, and the values are given in Figure 4.[19] It was found that the I_D/I_G ratio of pure SWCNTs was 0.5267, whereas after acid treatment (f-SWCNTs) the I_D/I_G value increased to 0.7317, confirming the successful functionalization of SWCNTs. In addition, positive shifts were observed in the D band (1342 to 1351 cm^{-1}) and the G band (1587 to 1591 cm^{-1}) of the f-SWCNTs. This is due to shortening of the SWCNTs as well as the creation of oxygen functional groups on the SWCNTs during the oxidative treatment, affording more anchoring sites for RuO_2NPs.[20] In fact, the oxygen functional groups make the SWCNTs hydrophilic and support homogeneous decoration and good adhesion of RuO_2NPs.[21] The calculated I_D/I_G ratio for RuO_2/SWCNT (0.1875) was low compared with that for f-SWCNTs (0.7317). This may be due to the reduction of the oxygen

functional groups during the calcination process.[19] Mainly, significant reduction of C−O−C, C=O, and COOH groups might lead to the reformation of SWCNTs from the f-SWCNTs, which is a probable reason for the lower I_D/I_G ratio of RuO_2/SWCNT (0.1875).[19c] Negative and positive shifts were also observed in the D band (1342 to 1331 cm^{-1}) and G band (1587 to 1593 cm^{-1}), respectively. The results revealed that the RuO_2NPs were strongly attached to the anchoring sites in the defect structure as well as in the prefect structure of SWCNTs.[20] This phenomenon might be due to the good dispersion of Ru(acac)$_3$ on f-SWCNTs during the grinding process.

XPS spectra were recorded for SWCNTs, f-SWCNTs, and RuO_2/SWCNT, and the results are shown in Figure 5. As expected, all three samples displayed C 1s and O 1s peaks at 284.4 and 532.5 eV, respectively (see Figure S3 in the Supporting Information).[21] Figure 5i,ii shows the deconvoluted C 1s and O 1s XPS spectra of f-SWCNTs, respectively. In the C 1s spectrum, the binding energies (BEs) of C−C/C=C, C−OH, C−O−C, C=O, and COOH groups are assigned as 284.3, 285.0, 285.8, 286.7, and 288.3 eV, respectively.[21] Likewise, deconvolution of the O 1s spectrum of f-SWCNTs resulted in five peaks located at 529.8, 530.7, 531.5, 532.2, and 533.5 eV, which were assigned to C=O, COOH, C−OH, C−O−C, and H_2O, respectively.[21] Moreover, in comparison with the C 1s spectrum of SWCNTs, the p → p* shakeup satellite peak at 291.5 eV completely disappeared in the spectrum of f-SWCNTs (inset of Figure 5i). FT-IR spectra (see Figure S4 in the Supporting Information) were also recorded for (a) SWCNTs and (a) f-SWCNTs to prove the creation of oxygen functional groups on the SWCNTs. Both samples showed a broad band at 3450 cm^{-1}, which corresponds to the stretching of the −OH group. In pure SWCNTs (a), the peaks observed at 2950 and 2830 cm^{-1} are ascribed to the asymmetric (ν_{as} CH_2) and symmetric (ν_s CH_2) stretching of the C−H bonds, and the typical peaks observed in the region from 1600 to 1350 cm^{-1} are due to the aromatic rings.[22] The intense band at 1725 cm^{-1} in the FT-IR spectrum of f-SWCNTs (b) can be assigned to the C=O stretching of carboxyl or carbonyl groups, and the peak appearing at 1210 cm^{-1} corresponds to the C−O−C stretching vibration. In addition, the band at 1570 cm^{-1} may be ascribed to the stretching of the carbon nanotube backbone.[22] In comparison with that for the pure SWCNTs, the intensity of the peak at 3450 cm^{-1} for the f-SWCNTs dramatically increased, which supports the formation of −COOH groups. These results confirm the successful creation of the oxygen functional groups on the SWCNTs. According to Fuller et al.,[23] the reactivity of SWCNTs is directly decided by the concentration of functional groups. The functional groups, mainly COOH, assist in creating good dispersion and adhesion of RuO_2NPs by replacement of the proton. In addition, the presence of functional groups facilitates exfoliation of the SWCNT bundles;[21] therefore, very high dispersion of RuO_2NPs on SWCNTs is obtained.

The XPS spectrum of RuO_2/SWCNT in the Ru 3p region (Figure 5iv) showed BE peaks for Ru 3p$_{3/2}$ at 462.5 eV and Ru 3p$_{1/2}$ at 485.2 eV, which are attributed to the photoemission from RuO_2 (Ru^{4+}).[24] Likewise, in the FT-IR spectrum of RuO_2/SWCNT (see Figure S5 in the Supporting Information), new peaks at around 700 cm^{-1} were observed compared with f-SWCNTs, which confirms the presence of Ru oxo species (most probably Ru^{4+} in RuO_2).[25,19b] Furthermore, the weight percentage of the elements present in the RuO_2/SWCNT was

Table 1. Screening for Optimal Reaction Conditions[a]
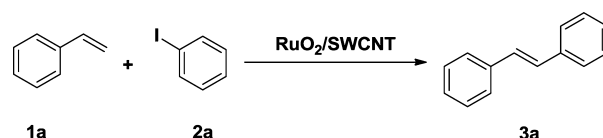
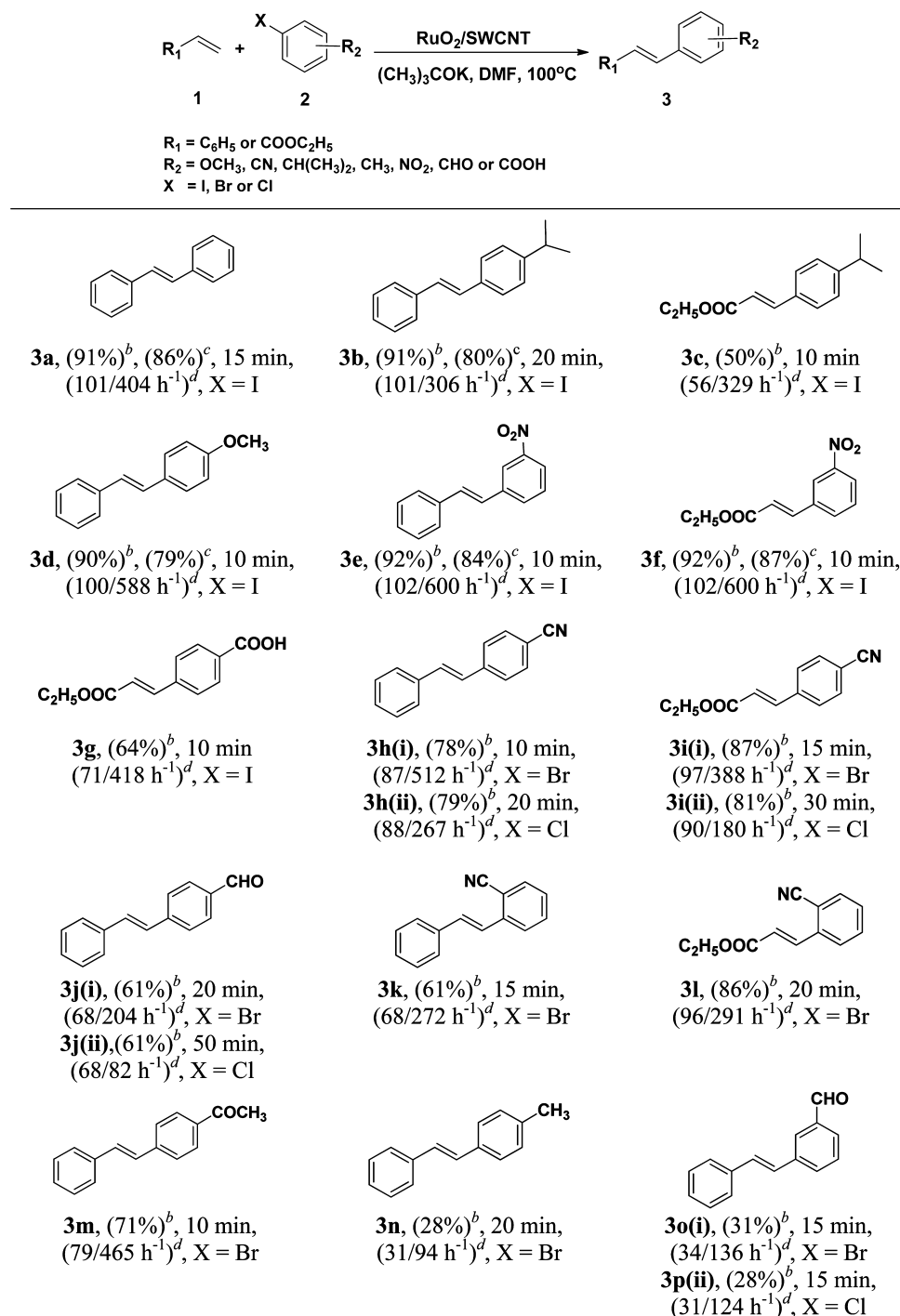| entry	solvent[b]	base	amount of base (mmol)	amount of catalyst (mol %)	temp. (°C)	time (min)	yield (%)[c]	TON/TOF (h^{-1})[d]
1	DMSO	(CH$_3$)$_3$COK	2.0	0.9	100	10	47	52/306
2	toluene	(CH$_3$)$_3$COK	2.0	0.9	100	10	32	36/212
3	**DMF**	**(CH$_3$)$_3$COK**	**2.0**	**0.9**	**100**	**10**	**91**	**101/594**
4	DMAc	(CH$_3$)$_3$COK	2.0	0.9	100	10	57	63/371
5	DMF	KOH	2.0	0.9	100	10	19	21/124
6	DMF	NaOH	2.0	0.9	100	10	39	43/253
7	DMF	K$_2$CO$_3$	2.0	0.9	100	10	55	61/359
8	DMF	NaOAc	2.0	0.9	100	10	14	16/94
9	DMF	(CH$_3$)$_3$COK	1.5	0.9	100	10	69	77/453
10	DMF	(CH$_3$)$_3$COK	2.5	0.9	100	10	90	100/529
11	DMF	(CH$_3$)$_3$COK	2.0	0.45	100	10	71	158/929
12	DMF	(CH$_3$)$_3$COK	2.0	1.35	100	10	91	67/394
13	DMF	(CH$_3$)$_3$COK	2.0	0.9	60	10	32	36/212
14	DMF	(CH$_3$)$_3$COK	2.0	0.9	80	10	56	62/365
15	DMF	(CH$_3$)$_3$COK	2.0	0.9	120	10	89	99/582
16	DMF	(CH$_3$)$_3$COK	2.0	0.9	100	5	78	87/975
17	DMF	(CH$_3$)$_3$COK	2.0	0.9	100	15	91	101/404
18	DMF	(CH$_3$)$_3$COK	2.0	0.9	100	20	91	101/306
19	DMF	(CH$_3$)$_3$COK	2.0	0.9	100	25	90	100/238
20	DMF	(CH$_3$)$_3$COK	2.0	0.9	100	30	91	101/202

[a]Reaction conditions: **1a** (3.0 mmol), **2a** (1.0 mmol), air atmosphere. [b]A 5 mL aliquot of solvent was used in all of the reactions. [c]GC yields. [d]The turnover number (TON) is defined as TON = (molar amount of product)/(molar amount of active sites). The turnover frequency (TOF) was calculated as TOF = TON/(time in h).

measured by XPS analysis. It is worth mentioning that only three elements (C, O, and Ru) were detected on the surface of RuO$_2$/SWCNT, and their weight percentages were 71.22 (C), 15.20 (O), and 13.58 (Ru). This result is in good agreement with the results of the SEM−EDS and ICP-MS analyses. The intensities of the peaks in both the O 1s and C 1s spectra of RuO$_2$/SWCNT dramatically decreased (Figure 5iii), indicating virtually complete reduction of the functional groups, as also revealed from the Raman spectra. Interestingly, the strong interaction of RuO$_2$NPs with SWCNTs was also confirmed by the positive shift in the C 1s peak of RuO$_2$/SWCNT compared with that of ƒ-SWCNTs (Figure 5iii). The crystalline structure of the Ru species in RuO$_2$/SWCNT was also confirmed by XRD (see Figure S6 in the Supporting Information). The very weak XRD peaks observed at 27.5°, 34.9°, 39.9°, and 57.5° correspond to the typical crystal faces (110), (101), (200), and (220), respectively, of RuO$_2$ (JCPDS no. 21-1172), confirming the nanocrystalline nature of the RuO$_2$.[26]

3.2. Screening for Optimal Reaction Conditions. Initially, the reaction of styrene (**1a**) with iodobenzene (**2a**) was chosen as the model reaction to screen the reaction conditions (Table 1). In this screening, reaction variables such as solvent, base, amount of base, amount of catalyst, temperature, and time were optimized to find the most effective reaction conditions. Among the various solvents tested, DMF was found to be most effective (Table 1, entries 1−4). It was found that (CH$_3$)$_3$COK was the most efficient base (Table 1, entries 3 and 5−8). The amount of base plays a crucial role in the efficiency of the present catalytic system, and 2.0 mmol of (CH$_3$)$_3$COK was found to be optimal (Table 1, entry 3). When the amount of base was decreased to 1.5 mmol,

the reaction was very slow (Table 1, entry 9). Unlike PdNP-based catalytic systems,[3,4] the drawback of the present catalytic system is the limitation on the use of weak and cheap bases such as KOH, NaOAc, and NaOH. The typical base K$_2$CO$_3$ gave the coupled product in moderate yield of 55%. Subsequently, the amount of catalyst was optimized (Table 1, entries 3, 11, and 12). A 5.0 mg loading of RuO$_2$/SWCNT (0.9 mol % Ru) was found to be the optimal amount of catalyst, affording an excellent yield of 91% (Table 1, entry 3). To our delight, this is the lowest loading of Ru catalyst (0.9 mol %) used to perform the Heck olefination of aryl halides. However, a further decrease in the catalyst loading to 0.45 mol % reduced the yield of the product to 71%; this might be due to an inadequate number of catalytically active species (Ru).[21d] In the temperature optimization (Table 1, entries 3 and 13−15), an excellent yield of 91% was obtained when the reaction mixture was stirred at 100 °C (Table 1, entry 3). To the best of our knowledge, among the Ru-based catalytic systems for Heck olefination of aryl halides, the present one requires the lowest reaction temperature. In the time optimization (Table 1, entries 3 and 16−20), a 91% yield of the product was obtained after 10 min. Further increases in the reaction time did not enhance the yield of the product. Moreover, under the optimized reaction conditions, the present catalytic system achieved a good yield of 91% with a good turnover number (TON) of 101 and turnover frequency (TOF) of 594 h^{-1} (Table 1, entry 3). The optimal reaction conditions were adopted to extend the scope of the Heck olefination of aryl halides.

3.3. Substrate Scope. As shown in Table 2, a wide range of aryl halides were effectively coupled to give the olefinated products in moderate to good yields. The product yield was

Table 2. Substrate Scope of the RuO$_2$/SWCNT-Catalyzed Heck-Type Olefination of Aryl Halides[a]

$$R_1 \diagup \!\!\!\! = \;\; + \;\; X\text{-}C_6H_4\text{-}R_2 \quad \xrightarrow[\text{(CH}_3)_3\text{COK, DMF, 100°C}]{\text{RuO}_2/\text{SWCNT}} \quad R_1\text{-}CH\!\!=\!\!CH\text{-}C_6H_4\text{-}R_2$$

1   **2**   **3**

R$_1$ = C$_6$H$_5$ or COOC$_2$H$_5$
R$_2$ = OCH$_3$, CN, CH(CH$_3$)$_2$, CH$_3$, NO$_2$, CHO or COOH
X   = I, Br or Cl

3a, (91%)[b], (86%)[c], 15 min,
(101/404 h^{-1})[d], X = I

3b, (91%)[b], (80%)[c], 20 min,
(101/306 h^{-1})[d], X = I

3c, (50%)[b], 10 min
(56/329 h^{-1})[d], X = I

3d, (90%)[b], (79%)[c], 10 min,
(100/588 h^{-1})[d], X = I

3e, (92%)[b], (84%)[c], 10 min,
(102/600 h^{-1})[d], X = I

3f, (92%)[b], (87%)[c], 10 min,
(102/600 h^{-1})[d], X = I

3g, (64%)[b], 10 min
(71/418 h^{-1})[d], X = I

3h(i), (78%)[b], 10 min,
(87/512 h^{-1})[d], X = Br
3h(ii), (79%)[b], 20 min,
(88/267 h^{-1})[d], X = Cl

3i(i), (87%)[b], 15 min,
(97/388 h^{-1})[d], X = Br
3i(ii), (81%)[b], 30 min,
(90/180 h^{-1})[d], X = Cl

3j(i), (61%)[b], 20 min,
(68/204 h^{-1})[d], X = Br
3j(ii),(61%)[b], 50 min,
(68/82 h^{-1})[d], X = Cl

3k, (61%)[b], 15 min,
(68/272 h^{-1})[d], X = Br

3l, (86%)[b], 20 min,
(96/291 h^{-1})[d], X = Br

3m, (71%)[b], 10 min,
(79/465 h^{-1})[d], X = Br

3n, (28%)[b], 20 min,
(31/94 h^{-1})[d], X = Br

3o(i), (31%)[b], 15 min,
(34/136 h^{-1})[d], X = Br
3p(ii), (28%)[b], 15 min,
(31/124 h^{-1})[d], X = Cl

[a]Reaction conditions: **1** (3.0 mmol), **2** (1.0 mmol), RuO$_2$/SWCNT (0.9 mol %), (CH$_3$)$_3$COK (2.0 mmol), DMF (5.0 mL), air atmosphere, 10−50 min, 100 °C. [b]GC yield. [c]Isolated yield. [d]TON/TOF.

fairly affected by various substituents on the aromatic ring of the aryl halide. Aryl iodides gave slightly higher yields than aryl bromides and aryl chlorides. In the olefination of iodobenzene with styrene, the present catalytic system gave a better yield of **3a** (91%) than the silylated Pd−NHC system.[27] The same reaction conditions were adopted to investigate the catalytic activity of our previously reported RuO$_2$-based catalyst (RuO$_2$/GNP).[26] The RuO$_2$/GNP catalyst gave a moderate yield of 67%, which may be due to the lower surface area of RuO$_2$/GNP (65.17 m^2 g^{-1}) compared with the present RuO$_2$/

SWCNT catalyst (415.77 m^2 g^{-1}). Interestingly, aryl iodides containing electron-donating groups such as CH(CH$_3$)$_2$ and OCH$_3$ at the para position were also effectively coupled with styrene to give the corresponding olefinated products **3b** and **3d** in excellent yields, whereas the same substrates exhibited lower yields with ethyl acrylate (**3c**). In the olefination of 1-iodo-3-nitrobenzene with styrene, an excellent 92% yield of **3e** was achieved. Similarly, the present system afforded a 92% yield of ethyl 3-(3-nitrophenyl)acrylate (**3f**) from the reaction of 1-iodo-3-nitrobenzene with ethyl acrylate. It was found that a

Scheme 1. Regioselectivity of the RuO$_2$/SWCNT-Catalyzed Heck Olefination Reaction
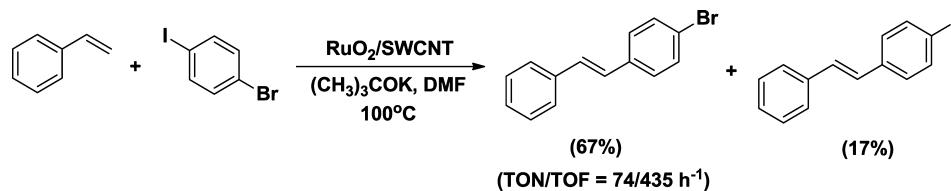
Scheme 2. Chemoselectivity of the RuO$_2$/SWCNT-Catalyzed Heck Olefination Reaction
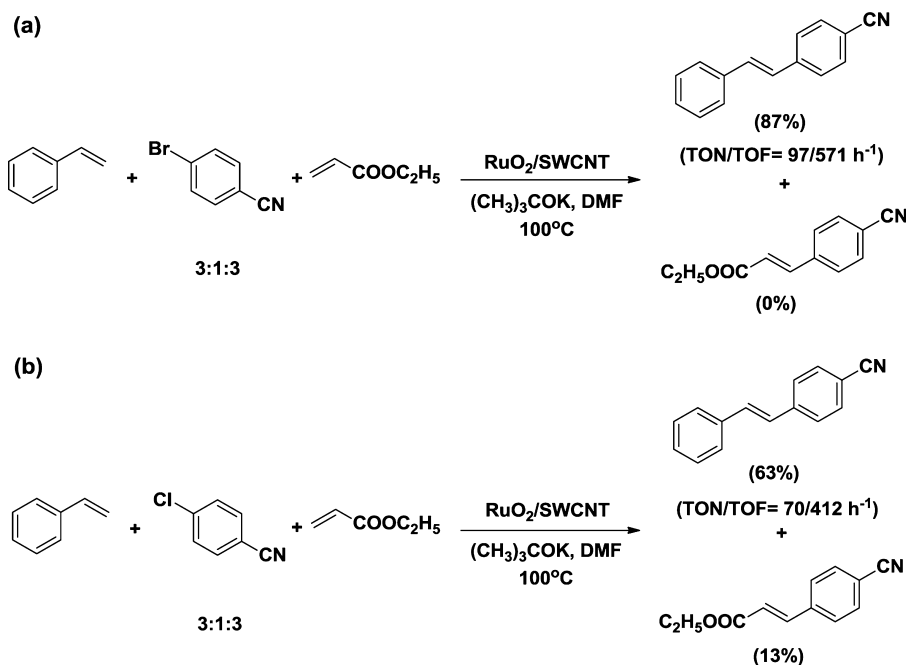
moderate 64% yield of **3g** was obtained in the coupling reaction of 1-iodo-4-benzoic acid with ethyl acrylate. The good yields obtained from aryl iodides are due to the better leaving ability of the iodo group.

The present catalytic system also worked well for the olefination of less reactive chloro- and bromoarenes. As shown in Table 2, a wide range of chloro- and bromoarenes were olefinated (**3h–o**). In particular, bromoarenes reacted faster than chloroarenes. For example, in the coupling of 4-bromobenzonitrile with styrene, the product **3h(i)** was obtained in 78% yield after just 10 min, whereas the coupling of 4-chlorobenzonitrile with styrene gave a 79% yield of the desired product **3h(ii)** only after 20 min. In the same way, an excellent 87% yield of ethyl 3-(4-cyanophenyl)acrylate [**3i(i)**] was achieved from the coupling of 4-bromobenzonitrile with ethyl acrylate in 15 min, but the similar olefination of 4-chlorobenzonitrile yielded only an 81% yield of **3i(ii)** after 30 min. The present RuO$_2$/SWCNT system gave a moderate 61% yield of **3j(i)** or **3j(ii)** in the coupling of 4-bromobenzaldehyde or 4-chlorobenzaldehyde with styrene. The present catalytic system required only 20 min to afford a 61% yield of the desired product **3k** from the coupling of 2-bromobenzonitrile with styrene, whereas the CuO/aluminosilicate system yielded the same product after 20 h.[6b] Interestingly, a good 86% yield of **3l** was obtained from the olefination of 2-bromobenzonitrile with ethyl acrylate. These results show the effectiveness of the present catalytic system toward the olefination of bromo- and chloroarenes. With a 0.9 mol % loading of RuO$_2$/SWCNT under optimal conditions, the olefination of 4-bromoacetophe-

none with styrene gave a better yield of **3m** (71%) compared with Pd-catalyzed coupling.[28] However, the olefination of the aryl bromide containing CH$_3$ at the para position afforded a lower yield of **3n** (28%). In the reactions of aryl halides containing a CHO group at the meta position to afford **3o(i)** and **3o(ii)**, the GC analyses showed the presence of side products: bromo- or chlorobenzoic acid and styrylbenzoic acid. Importantly, for the Ru-catalyzed Heck coupling reactions, the present TONs (31–101) and TOFs (94–600 h^{-1}) are the highest reported to date. The excellent catalytic activity of RuO$_2$/SWCNT is due to three most important reasons: (i) the ultrafine nature of the RuO$_2$NPs, (ii) high specific surface area of RuO$_2$/SWCNT, and (iii) effective dispersion of RuO$_2$/SWCNT in the reaction medium.

3.4. Regio- and Chemoselectivity. To study the regioselectivity of the present catalytic system, the coupling between styrene and 1-bromo-4-iodobenzene was carried out under the optimized reaction conditions (Scheme 1). As expected, 1-bromo-4-styrylbenzene was selectively formed in 67% yield with a higher TON (74) and TOF (435 h^{-1}), whereas only a 17% yield of 1-iodo-4-styrylbenzene was obtained. This can be explained by the better leaving ability of the iodo group compared with the bromo group.

When a mixture of styrene (3 mmol), ethyl acrylate (3.0 mmol), and either 4-bromobenzonitrile (Scheme 2a) or 4-chlorobenzonitrile (Scheme 2b) (1.0 mmol) was allowed to stir under the optimized reaction conditions, the aryl halide selectively coupled with styrene to give 4-styrylbenzonitrile in good yield with higher TON (97/70) and TOF (571/412 h^{-1})
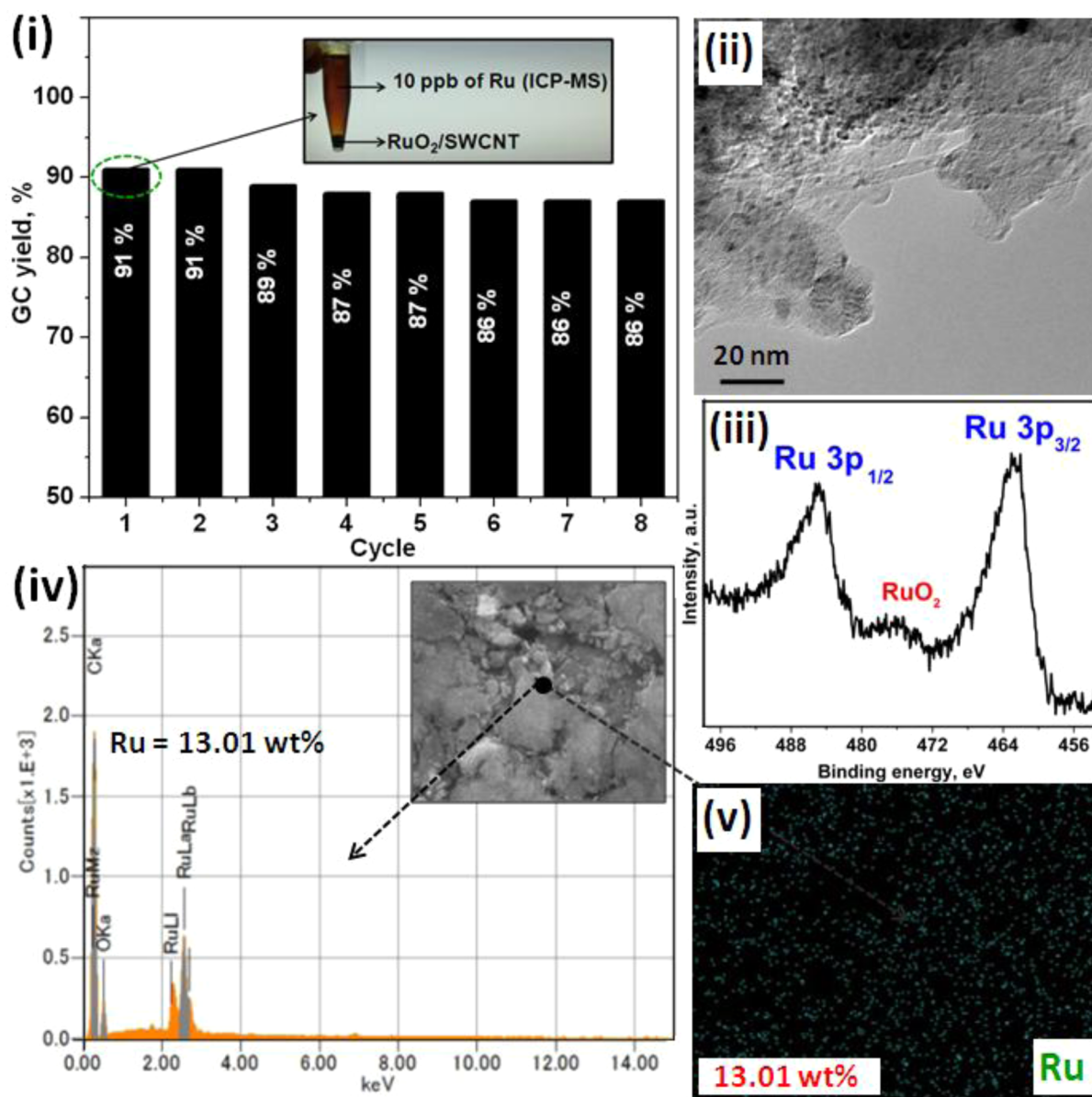
Figure 6. (i) Heterogeneity and recyclability test of RuO$_2$/SWCNT [styrene (343 μL, 3.0 mmol), iodobenzene (111 μL, 1.0 mmol), (CH$_3$)$_3$COK (224 mg, 2.0 mmol) and RuO$_2$/SWCNT (5 mg, 0.9 mol % of Ru) at 100 °C in 5 mL of DMF], (ii) TEM image, (iii) Ru 3p XPS spectrum, (iv) SEM and corresponding EDS spectrum of u-RuO$_2$/SWCNT, and (v) corresponding EDS mapping of Ru.

in the presence of ethyl acrylate. These results prove the chemoselective nature of the RuO$_2$/SWCNT catalytic system.

3.5. Heterogeneity, Reusability, and Stability of RuO$_2$/SWCNT. It is well-known that several heterogeneous catalysts, particularly in Heck-type olefination reactions, suffer from leaching of the active species from the support, and therefore, the stability and reusability of the catalysts are highly limited. To check whether the RuO$_2$ active species leached out of the SWCNT support during the reaction, a heterogeneity test was performed. In a typical test, a mixture of styrene (343 μL, 3.0 mmol) and iodobenzene (111 μL, 1.0 mmol) was stirred under the optimized reaction conditions. After the reaction was completed, the solid RuO$_2$/SWCNT was separated from the reaction mixture by centrifugation and then the filtrate was analyzed by ICP-MS (Figure 6i); a very low content of Ru (~10 ppb) confirmed that the leaching of active species (RuO$_2$) from the SWCNT support was negligible. This result inspired a subsequent investigation of the reusability of the

catalyst. After the first use, the catalyst was separated by centrifugation, washed, dried at 60 °C, and then reused. The catalyst was reused eight times, and the yields of product are shown in Figure 6i. The merit of the proposed catalytic system can be realized from the reusability of RuO$_2$/SWCNT, which showed an excellent yield (86%), TON (96), and TOF (565 h^{-1}) in the eighth cycle. Moreover, to confirm the stability of the catalyst, after the first use, the used RuO$_2$/SWCNT (u-RuO$_2$/SWCNT) was analyzed by TEM, XPS, and SEM—EDS (Figure 6ii—v). It can be seen that no significant change in the morphology of u-RuO$_2$/SWCNT was found compared with the fresh RuO$_2$/SWCNT. The oxidation state and weight percentage of Ru in u-RuO$_2$/SWCNT were found to be +4 and 13.01 wt %, respectively. These results indicate that RuO$_2$/SWCNT is physically as well as chemically stable. However, the TEM image of the catalyst after the eighth cycle (see Figure S7 in the Supporting Information) shows a significant change in the morphology compared with the fresh RuO$_2$/SWCNT. In
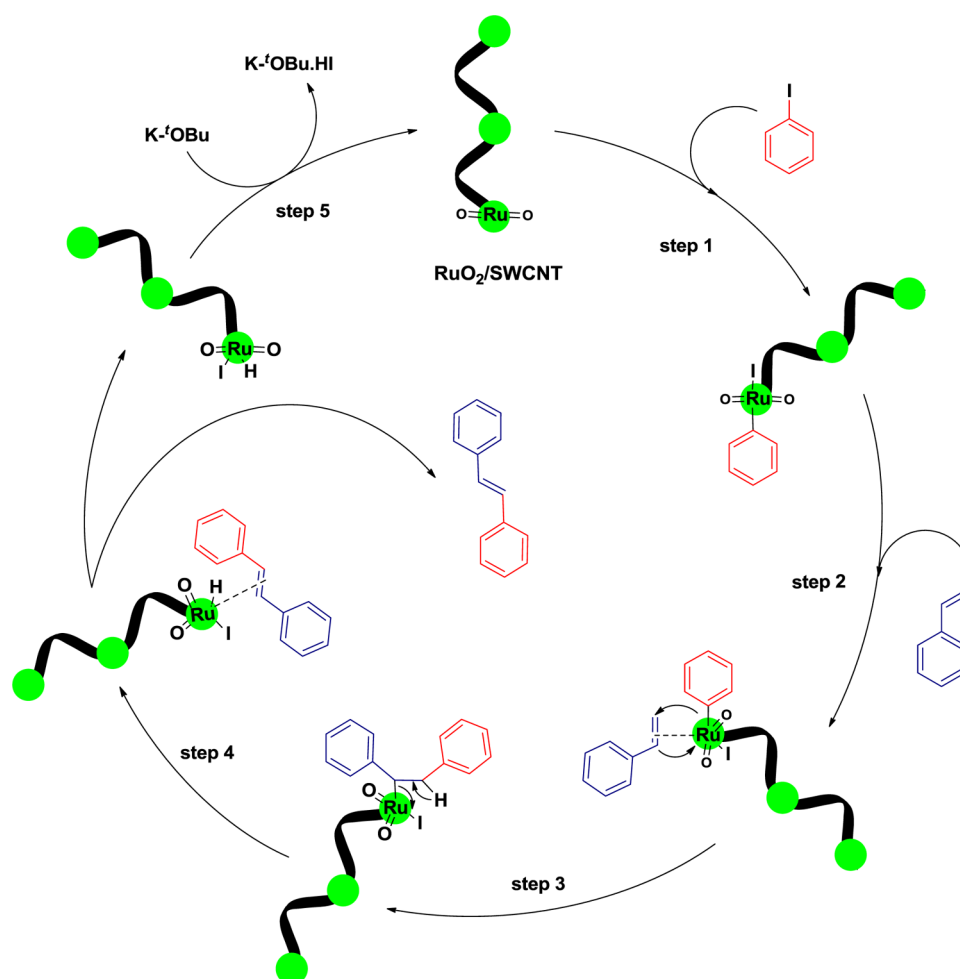
Figure 7. Proposed mechanism for the Heck olefination of iodobenzene with styrene.

particular, the mean diameter of the RuO$_2$NPs increased (from 0.9 to 6.1 nm) with aggregation of the RuO$_2$NPs. On the contrary, no significant changes in the oxidation state and weight percentage of Ru were found. This might be the reason for the slight decrease in the yield of the coupled product (from 91 to 86%) in the eighth cycle.

3.6. Proposed Mechanism. In order to understand the mechanism of the RuO$_2$/SWCNT-catalyzed Heck olefination of aryl halides, FT-IR and XPS spectra (see Figures S8−S10 in the Supporting Information) were recorded for RuO$_2$/SWCNT (the pure nanocatalyst), h-RuO$_2$/SWCNT (the catalyst after stirring with iodobenzene in 5 mL of DMF at 100 °C for 5 min), and u-RuO$_2$/SWCNT (the used nanocatalyst). In comparison with pure RuO$_2$/SWCNT, h-RuO$_2$/SWCNT showed extra peaks in both the FT-IR and C 1s XPS spectra, which may be attributed to adsorption of the aryl halide on the active sites of RuO$_2$NPs. Furthermore, the XPS spectrum of h-RuO$_2$/SWCNT showed new peaks in the I 3p region (see Figure S9ii in the Supporting Information).[29a] A positive shift in the Ru 2p$_{3/2}$ peak (see Figure S9iii in the Supporting Information) was also observed. Recently, in their experimental investigation of the redox properties of RuO$_2$NPs decorated on single-layer graphene, Soin and co-workers[29b] confirmed the formation of high-valent Ru species such as Ru(VI) and Ru(VIII) on the RuO$_2$NPs surface by XPS analysis. Likewise, in the present case, the positive shift in the Ru 2p$_{3/2}$ peak might be due to a change in the oxidation state of RuO$_2$NPs from

Ru(IV) to Ru(VI) by an addition reaction of aryl halide species with RuO$_2$NPs supported on SWCNTs. The XPS spectrum of u-RuO$_2$/SWCNT (see Figure S10 in the Supporting Information) confirmed the formation of K-^{t}OBu·HI (I 3p and K 2p XPS spectrum) during the reaction. Moreover, after the reaction, the organic layer was separated out and analyzed by ICP-MS; a negligible amount of Ru (∼10 ppb) leached from the catalyst during the reaction.

On the basis of the results obtained from the XPS, ICP-MS and FT-IR analyses, we concluded that the catalytic reaction might take place on the RuO$_2$NPs surface via oxidative addition followed by reductive elimination (Figure 7). In step 1, the aryl halide is oxidatively added to the Ru(IV) of the RuO$_2$NPs surface to form a Ru(VI) complex. In step 2, alkyl insertion into the Ru(VI)−π complex takes place, forming the Ru(VI)−σ complex intermediate (step 3). Subsequently, in step 4 the intermediate is converted into the product by β-hydride elimination. Finally, RuO$_2$/SWCNT is regenerated after the HI elimination in the presence of K-^{t}OBu (step 5).

4. CONCLUSIONS

In conclusion, a highly efficient SWCNT-supported RuO$_2$NP-based catalytic system for the Heck olefination of aryl halides has been developed. The reaction could be efficiently carried out with as low as a 0.9 mol % loading of the supported RuO$_2$ catalyst over a wide range of substrates in moderate to excellent yields with good TON and TOF values. In addition to the

iodoarenes, less reactive bromo- and chloroarenes could also be effectively olefinated using the present catalytic system. To the best of our knowledge, RuO_2/SWCNT is the most active Ru-based heterogeneous catalyst for the Heck olefination of aryl halides among those reported to date. RuO_2/SWCNT is highly regioselective and chemoselective for the Heck olefination reaction. The heterogeneity and reusability of RuO_2/SWCNT were found to be good. Overall, the simple synthesis and excellent activity make RuO_2/SWCNT an alternative to the existing Ru-based catalysts for Heck coupling reactions.

■ ASSOCIATED CONTENT

Ⓢ Supporting Information

TEM and corresponding elemental mapping images, an XRD pattern, FT-IR and XPS spectra, and NMR data for selected products. This material is available free of charge via the Internet at http://pubs.acs.org.

■ AUTHOR INFORMATION

Corresponding Authors
*Phone: +91 431 2503636. E-mail: kar@nitt.edu.
*Phone: +81 268 21 5139. E-mail: kim@shinshu-u.ac.jp.

Notes
The authors declare no competing financial interest.

■ ACKNOWLEDGMENTS

■ REFERENCES

(1) (a) *Metal-Catalyzed Cross-Coupling Reactions*; Diederich, F., Stang, P. J., Eds.; Wiley-VCH: Weinheim, Germany, 1998. (b) Baur, J. A.; Sinclair, D. A. *Nat. Rev. Drug Discovery* **2006**, *5*, 493−506.

(2) (a) Beletskaya, I. P.; Cheprakov, A. V. *Chem. Rev.* **2000**, *100*, 3009−3066. (b) Whitcombe, N. J.; Hii, K. K.; Gibson, S. E. *Tetrahedron* **2001**, *57*, 7449−7476. (c) Blaser, H. U.; Indolese, A.; Naud, F.; Nettekoven, U.; Schnyder, A. *Adv. Synth. Catal.* **2004**, *346*, 1812−1817. (d) Shaughnessy, K. H.; Kim, P.; Hartwig, J. F. *J. Am. Chem. Soc.* **1999**, *121*, 2123−2132. (e) Littke, A. F.; Fu, G. C. *J. Am. Chem. Soc.* **2001**, *123*, 6989−7000.

(3) (a) Okamoto, K.; Akiyama, R.; Yoshida, H.; Yoshida, T.; Kobayashi, S. *J. Am. Chem. Soc.* **2005**, *127*, 2125−2135. (b) Dahan, A.; Portnoy, M. *Org. Lett.* **2003**, *5*, 1197−1200. (c) Yang, Y.-C.; Luh, T.-Y. *J. Org. Chem.* **2003**, *68*, 9870−9873. (d) Garcia-Martinez, J. C.; Lezutekong, R.; Crooks, R. M. *J. Am. Chem. Soc.* **2005**, *127*, 5097−5103. (e) Calo, V.; Nacci, A.; Monopoli, A.; Fornaro, A.; Sabbatini, L.; Cioffi, N.; Ditaranto, N. *Organometallics* **2004**, *23*, 5154−5158. (f) Huang, J.; Jiang, T.; Gao, H.; Han, B.; Liu, Z.; Wu, W.; Chang, Y.; Zhao, G. *Angew. Chem., Int. Ed.* **2004**, *43*, 1397−1399. (g) Desforges, A.; Backov, R.; Deleuze, H.; Mondain-Monval, O. *Adv. Funct. Mater.* **2005**, *15*, 1689−1695. (h) Arvela, R. K.; Leadbeater, N. E.; Sangi, M. S.; Williams, V. A.; Granados, P.; Singer, R. D. *J. Org. Chem.* **2005**, *70*, 161−168. (i) Kleist, W. *Catal. Lett.* **2008**, *125*, 197−200.

(4) For recent reviews and reports, see: (a) Crudden, C. M.; Sateesh, M.; Lewis, R. *J. Am. Chem. Soc.* **2005**, *127*, 10045−10050. (b) Kwon, M. S.; Kim, N.; Park, C. M.; Lee, J. S.; Kang, K. Y.; Park, J. *Org. Lett.* **2005**, *7*, 1077−1079. (c) McNamara, C. A.; Dixon, M. J.; Bradley, M. *Chem. Rev.* **2002**, *102*, 3275−3299. (d) Brase, S.; Kirchhoff, J. H.; Kobberling, J. *Tetrahedron* **2003**, *59*, 885−939. (e) Denmark, S. E.; Sweis, R. F. *Acc. Chem. Res.* **2002**, *35*, 835−846. (f) Narayanan, R.; El-Sayed, M. A. *Langmuir* **2005**, *21*, 2027−2033. (g) Teranishi, T.; Miyake, M. *Chem. Mater.* **1998**, *10*, 594−600. (h) De Vries, J. G.

Dalton Trans. **2006**, 421−429. (i) Evangelisti, C.; Panziera, N.; D'Alessio, A.; Bertinetti, L.; Botavina, M.; Vitulli, G. *J. Catal.* **2010**, *272*, 246−252. (j) Mieczynska, E.; Gnieweka, A.; Zawadzki, M. *Appl. Catal., A* **2011**, *393*, 195−205. (k) Martins, D. L.; Alvarez, H. M.; Aguiar, L. C. S. *Tetrahedron Lett.* **2010**, *51*, 6814−6817. (l) Makhubela, B. C. E.; Jardine, A.; Smith, G. S. *Appl. Catal., A* **2011**, *393*, 231−240. (m) Farrauto, R. J.; Bartholomew, C. H. *Fundamentals of Industrial Catalytic Processes*, 1st ed.; Blackie Academic and Professional: London, 1997; p 351.

(5) (a) Mehnert, C. P.; Ying, J. Y. *Chem. Commun.* **1997**, 2215−2216. (b) Ioni, Y. V.; Lyubimov, S. E.; Davankov, V. A.; Gubin, S. P. *Russ. J. Inorg. Chem.* **2013**, *58*, 392−394.

(6) (a) Iyer, S.; Ramesh, C.; Sarkar, A.; Wadgaonkar, P. P. *Tetrahedron Lett.* **1997**, *38*, 8113−8116. (b) Ganesh Babu, S.; Neelakandeswari, N.; Dharmaraj, N.; Jackson, S. D.; Karvembu, R. *RSC Adv.* **2013**, *3*, 7774−7781.

(7) (a) Lipshutz, B. H.; Sclafani, J. A.; Blomgren, P. A. *Tetrahedron* **2000**, *56*, 2139−2144. (b) Saito, S.; Oh-tani, S.; Miyaura, N. *J. Org. Chem.* **1997**, *62*, 8024−8030.

(8) Furstner, A.; Leitner, A.; Mendez, M.; Krause, H. *J. Am. Chem. Soc.* **2002**, *124*, 13856−13863.

(9) (a) Lautens, M.; Roy, A.; Fukuoka, K.; Fagnou, K.; Martın-Matute, B. *J. Am. Chem. Soc.* **2001**, *123*, 5358−5359. (b) Oi, S.; Honma, Y.; Inoue, Y. *Org. Lett.* **2002**, *4*, 667−669.

(10) (a) Koike, T.; Du, X.; Sanada, T.; Danda, Y.; Mori, A. *Angew. Chem., Int. Ed.* **2003**, *42*, 89−92. (b) Iyer, S. *J. Organomet. Chem.* **1995**, *490*, 27−28.

(11) (a) Houdayer, A.; Schneider, R.; Billaud, D.; Ghanbaja, J.; Lambert, J. *Synth. Met.* **2005**, *151*, 165−174. (b) Miao, S.; Zhang, C.; Liu, Z.; Han, B.; Xie, Y.; Ding, S.; Yang, Z. *J. Phys. Chem. C* **2008**, *112*, 774−780.

(12) (a) Naota, T.; Takaya, H.; Murahashi, S. I. *Chem. Rev.* **1998**, *98*, 2599−2660. (b) Veerakumar, P.; Ramdass, A.; Rajagopal, S. *J. Nanosci. Nanotechnol.* **2013**, *13*, 4761−4786. (c) Kantam, M. L.; Reddy, R. S.; Pal, U.; Sudhakar, M.; Venugopal, A.; Ratnam, K. J.; Figueras, F.; Chintareddy, V. R.; Nishina, Y. *J. Mol. Catal. A: Chem.* **2012**, *359*, 1−7. (d) Yamaguchi, K.; Mizuno, N. *Chem.—Eur. J.* **2003**, *9*, 4353−4361. (e) Zhao, C.; Luo, C.; Dyson, P. J.; Liu, H.; Kou, Y. *J. Am. Chem. Soc.* **2006**, *128*, 8714−8715. (f) Sarmah, P. P.; Dutta, D. K. *Green Chem.* **2012**, *14*, 1086−1093. (g) Shi, F.; Tse, M. K.; Zhou, S.; Pohl, M. M.; Radnik, J.; Hubner, S.; Jahnisch, K.; Bruckner, A.; Beller, M. *J. Am. Chem. Soc.* **2009**, *131*, 1775−1779. (h) Concepcion, J. J.; Jurss, J. W.; Norris, M. R.; Chen, Z.; Templeton, J. L.; Meyer, T. J. *Inorg. Chem.* **2010**, *49*, 1277−1279. (i) Zhan, B. Z.; White, M. A.; Sham, T. K.; Pincock, J. A.; Doucet, R. J.; Rao, K. V. R.; Robertson, K. N.; Cameron, T. S. *J. Am. Chem. Soc.* **2003**, *125*, 2195−2199. (j) Yin, S. F.; Xu, B. Q.; Ng, C. F.; Au, C. T. *Appl. Catal., B* **2004**, *48*, 237−241. (k) Miao, S.; Liu, Z.; Han, B.; Huang, J.; Sun, Z.; Zhang, J.; Jiang, T. *Angew. Chem., Int. Ed.* **2006**, *45*, 266−269. (l) Miyazaki, A.; Balint, I.; Aika, K.; Nakano, Y. *J. Catal.* **2001**, *204*, 364−371.

(13) (a) Naota, T.; Takaya, H.; Murahashi, S. I. *Chem. Rev.* **1998**, *98*, 2599−2600. (b) Mitsudo, T. A.; Kondo, T. *Synlett* **2001**, 309−321. (c) Trost, B. M.; Toste, F. D.; Pinkerton, A. B. *Chem. Rev.* **2001**, *101*, 2067−2096. (d) Mitsudo, T. A.; Takagi, M.; Zhang, S. W.; Watanabe, Y. *J. Organomet. Chem.* **1992**, *423*, 405−414. (e) Ritleng, V.; Sirlin, C.; Pfeffer, M. *Chem. Rev.* **2002**, *102*, 1731−1769.

(14) Na, Y.; Park, S.; Han, S. B.; Han, H.; Ko, S.; Chang, S. *J. Am. Chem. Soc.* **2004**, *126*, 250−258.

(15) (a) Joo, S. H.; Park, J. Y.; Renzas, J. R.; Butcher, D. R.; Huang, W. Y.; Somorjai, G. A. *Nano Lett.* **2010**, *10*, 2709−2713. (b) Lu, J.; Do, I.; Drzal, L. T.; Worden, R. M.; Lee, I. *ACS Nano* **2008**, *2*, 1825−1832.

(16) (a) Gómez-Escalonilla, M. J.; Atienzar, P.; Garcia Fierro, J. L.; García, H.; Langa, F. *J. Mater. Chem.* **2008**, *18*, 1592−1600. (b) Wu, G.; Chen, Y. S.; Xu, B. Q. *Electrochem. Commun.* **2005**, *7*, 1237−1243.

(17) Krasheninnikov, A. V.; Lehtinen, P. O.; Foster, A. S.; Pyykko, P.; Nieminen, R. M. *Phys. Rev. Lett.* **2009**, *102*, No. 126807.

(18) (a) Tsang, S. C.; Chen, Y. K.; Harris, P. J. F.; Green, M. L. H. *Nature* **1994**, *372*, 159−162. (b) Stetzenbach, K. J.; Amano, M.; Kreamer, D. K.; Hodge, V. F. *Ground Water* **1994**, *32*, 976−985.

(19) (a) Dresselhaus, M. S.; Dresselhaus, G.; Saito, R.; Jorio, A. *Phys. Rep.* **2005**, *409*, 47−99. (b) Gopiraman, M.; Ganesh Babu, S.; Khatri, Z.; Kai, W.; Kim, A. Y.; Endo, M.; Karvembu, R.; Kim, I. S. *J. Phys. Chem. C* **2013**, *117*, 23582−23596. (c) Fan, X.; Peng, W.; Li, Y.; Li, X.; Wang, S.; Zhang, G.; Zhang, F. *Adv. Mater.* **2008**, *20*, 4490−4493.

(20) (a) Simmons, T. J.; Bult, J.; Hashim, D. P.; Linhardt, R. J.; Ajayan, P. M. *ACS Nano* **2009**, *3*, 865−870. (b) Datsyuk, V.; Kalyva, M.; Papagelis, K.; Parthenios, J.; Tasis, D.; Siokou, A.; Kallitsis, I.; Galiotis, C. *Carbon* **2008**, *46*, 833−840. (c) Souza Filho, A. G.; Meunier, V.; Terrones, M.; Sumpter, B. G.; Barros, E. B.; Villalpando-Paez, F.; Filho, J. M.; Kim, Y. A.; Muramatsu, H.; Hayashi, T.; Endo, M.; Dresselhaus, M. S. *Nano Lett.* **2007**, *7*, 2383−2388.

(21) (a) Akhavan, O. *Carbon* **2010**, *48*, 509−519. (b) Kuila, T.; Bhadra, S.; Yao, D.; Kim, N. H.; Bose, S.; Lee, J. H. *Prog. Polym. Sci.* **2010**, *35*, 1350−1375. (c) Kumar, V. A.; Aswathy, T. V.; Periyasamy, K.; Thirumalaiswamy, R. *Green Chem.* **2013**, *15*, 3259−3267. (d) Gopiraman, M.; Ganesh Babu, S.; Khatri, Z.; Kai, W.; Kim, A. Y.; Endo, M.; Karvembu, R.; Kim, I. S. *Carbon* **2013**, *62*, 135−148.

(22) Li, G. Y.; Wang, P. M.; Zhao, X. *Carbon* **2005**, *43*, 1239−1245. (b) Motchelaho, M. A. M.; Xiong, H.; Moyo, M.; Jewell, L. L.; Coville, N. J. *J. Mol. Catal. A: Chem.* **2011**, *335*, 189−198. (c) Vinayan, B. P.; Nagar, R.; Raman, V.; Rajalakshmi, N.; Dhathathreyan, K. S.; Ramaprabhu, S. *J. Mater. Chem.* **2012**, *22*, 9949−9956. (d) Tu, X.; Luo, X.; Luo, S.; Yan, L.; Zhang, F.; Xie, Q. *Microchim. Acta* **2010**, *169*, 33−40.

(23) *Proton Exchange Membrane Fuel Cells 8*; Fuller, T., Shinohara, K., Ramani, V., Shirvanian, P., Uchida, H., Cleghorn, S., Inaba, M., Mitsushima, S., Strasser, P., Nakagawa, H., Gasteiger, H., Zawodzinski, T., Lamy, C., Eds.; ECS Transactions, Vol. *16*, Issue 2; The Electrochemical Society: Pennington, NJ, 2008.

(24) Chakroune, N.; Viau, G.; Ammar, S.; Poul, L.; Veautier, D.; Chehimi, M. M.; Mangeney, C.; Villain, F.; Fievet, F. *Langmuir* **2005**, *21*, 6788−6796.

(25) (a) Saburo, H.; Satoshi, N.; Makoto, T.; Kazunori, U.; Hiroyoshi, K.; Seiichiro, I. *Appl. Catal., A* **2005**, *288*, 67−73. (b) Chi, M. C.; Ting, F. L.; Kwok, Y. W. *Inorg. Chem.* **1987**, *26*, 2289−2299. (c) Gopiraman, M.; Bang, H.; Ganesh Babu, S.; Wei, K.; Karvembu, R.; Kim, I. S. *Catal. Sci. Technol.* **2014**, DOI: 10.1039/C3CY00963G.

(26) Gopiraman, M.; Ganesh Babu, S.; Khatri, Z.; Kai, W.; Endo, M.; Karvembu, R.; Kim, I. S. *Catal. Sci. Technol.* **2013**, *3*, 1485−1495.

(27) Polshettiwar, V.; Hesemann, P.; Moreau, J. J. E. *Tetrahedron Lett.* **2007**, *48*, 5363−5366.

(28) Palmisano, G.; Bonrath, W.; Boffa, L.; Garella, D.; Barge, A.; Cravotto, G. *Adv. Synth. Catal.* **2007**, *349*, 2338−2344.

(29) (a) Kiel, S.; Grinberg, O.; Perkas, N.; Charmet, J.; Kepner, H.; Gedanken, A. *Beilstein J. Nanotechnol.* **2012**, *3*, 267−276. (b) Soin, N.; Roy, S. S.; Mitra, S. K.; Thundat, T.; McLaughlin, J. A. *J. Mater. Chem.* **2012**, *22*, 14944−14950.